Drastic effects of vacancies on phonon lifetime and thermal conductivity in graphene

G Bouzerar, S Thébaud, S Pecorario, Ch Adessi

Drastic effects of vacancies on phonon lifetime and thermal conductivity in graphene

G. Bouzerar[1], S. Thébaud[1], S. Pecorario[1] and Ch. Adessi[1]

[1] CNRS et Université Lyon 1, 6, rue Ada Byron, 69622 Villeurbanne Cedex, France

(Dated: February 26, 2020)

Understanding thermal transport in 2D materials and especially in graphene is a key challenge for the design of heat management and energy conversion devices. The high sensitivity of measured transport properties to structural defects, ripples and vacancies is of crucial importance in these materials. Using a first principle based approach combined with an exact treatment of the disorder, we address the impact of vacancies on phonon lifetimes and thermal transport in graphene. We find that perturbation theory fails completely and overestimates phonon lifetimes by almost two orders of magnitude. Whilst, in defected graphene, LA and TA modes remain well defined, the ZA modes become marginal. In the long wavelength limit, the ZA dispersion changes from quadratic to linear and the scattering rate is found proportional to the phonon energy, in contrast to the quadratic scaling often assumed. The impact on thermal transport, calculated beyond the relaxation time approximation and including first principle phonon-phonon scattering rates as reported recently for pristine graphene, reveals spectacular effects even for extremely low vacancy concentrations.

PACS numbers:

I. INTRODUCTION

Over the past decade, and because of its unique mechanical, electronic, optical and thermal properties, the 2D material prototype, graphene, has been at the heart of a plethora of publications.[1–3] Among all these remarkable properties, the particular topic of thermal transport has attracted much attention over the past years. Graphene exhibits an unusually high thermal conductivity,[4–7] that could, in the near future, make this two dimensional material one of the best candidates for efficient thermal dissipation in microelectronics. In addition, nanostructuring[8] and disorder[9] in graphene based compounds could be promising pathways for high-efficiency thermoelectric devices to transform waste heat into electrical energy. The desired effects are a drastic suppression of the thermal conductivity and significant improvement of the Seebeck coefficient, both required to reach a large thermoelectric efficiency.

Many efforts are still devoted to understanding the lattice thermal conductivity in graphene, but no clear consensus has been reached so far, the topic remains controversial. Experimentally, the measured room temperature thermal conductivity (κ) spans over a large range of values, typically between 400 W.m.$^{-1}$K^{-1} and 600 W.m.$^{-1}$K^{-1} for supported samples[6,10] and 1500 W.m.$^{-1}$K^{-1} to 5400 W.m.$^{-1}$K^{-1} for suspended ones.[4,6,11] The important fluctuations in the measured values can be attributed to (i) large measurement uncertainties, (ii) variations in the processing conditions and (iii) graphene quality. This could indicate a high sensitivity to intrinsic defects such as vacancies, lattice reconstruction, edge roughness or even ripples. From the theoretical side,[12–19] the scenario is even more open. The estimates of κ at room temperature in graphene vary by more than one order of magnitude, typically it ranges from 500 W.m.$^{-1}$K^{-1} to about 9000 W.m.$^{-1}$K^{-1}. Even, the choice of exchange correlation functional has a sig-

nificant impact on the thermal conductivity in pristine graphene[19].

It is well-known that a plethora of intrinsic defects are possible in graphene, such as isotopes, vacancies and divacancies, Stone-Wales defects... Molecular dynamics simulations have been the standard and most widely used tool to address their effects on the thermal conductivity of graphene, carbon nanotubes and other complex carbon allotropes[20–24]. However, we choose here an alternative approach (presented below) in order to focus on the influence of defects on the nature and lifetime of individual phonon modes. Because we expect vacancies to have the strongest effects on thermal transport, we focus our study on this type of defect.

In this paper, using state of the art first principle based approaches, we address the issue of vacancies' effects on lattice thermal transport in single mono-layer graphene. For that purpose, we follow a two steps procedure. First, we calculate the vacancy induced multiple scattering contribution to the phonon lifetime by an exact real space treatment of the disorder. Notice that, in most of the existing theoretical studies, disorder is treated perturbatively. As will be seen, the second order perturbation theory appears to severely overestimate the phonon lifetimes. Note however, that the perturbation theory often used in the case of isotopic disorder is reasonable, because of the weak effects of the substitution of ^{12}C by ^{13}C. In the second step, we calculate the thermal conductivity as a function of the vacancy concentration by including phonon-phonon scattering (Normal and Umklapp processes) and going beyond the relaxation time approximation (RTA). It should be emphasized that all calculations are parameter free, since the disordered phonon dynamical matrix is obtained from first principle calculations. Note that, within a single site T-matrix approach, the issue of phonon lifetime in graphene in the presence of various dopant (B,N,P) and vacancies has been recently adressed in Ref. 26. In contrast, here we treat the disor-

der exactly (finite concentration of randomly distributed vacancies) and thus properly include the multiple scatterings of the phonon modes and the localization physics. In addition, we focus our attention on the vacancy concentration dependence of both phonon dispersion and lifetime in the long wave length limit and address quantitatively the validity of the often used second order perturbation theory. The energy dependence of the phonon lifetime is directly extracted from an accurate calculation of the averaged (over disorder configurations) dynamical spectral function. We should emphasize that our accurate treatment of the disorder yields an unexpected power law for the ZA scattering rate that had not been revealed so far.

II. EXACT DISORDER CONTRIBUTION TO THE PHONON LIFETIME

Fig. 1(left) shows the calculated dispersion in the pristine graphene monolayer along the Γ-M-K-Γ path in the Brillouin Zone (BZ). The inter-atomic force constants (IFC) $\phi_{\mathbf{ij}}^{\alpha\beta}$ have been calculated from first principle simulations, $\mathbf{i}$ and $\mathbf{j}$ are the positions of the C atoms and α, β = x, y and z. The *ab initio* calculations of the IFC are performed with the DFT package SIESTA,[25] more details are provided in the Appendix. Note that in the case of graphene, in-plane (xy) and out of plane (z) modes are decoupled. We observe an excellent agreement between our calculations and the experimental data, over the whole BZ. We should emphasize that, we have retained the first 6 nearest neighbour shells for the calculations, including further shells has negligible effects.

In Fig. 1(middle) are plotted the nearest-neighbour inter-atomic force constants ϕ_{n-n}^{zz} for the out of plane modes (ZA and ZO) in the vicinity of a vacancy. The rectangular supercell used for the calculations contains 199 C atoms. In a pure graphene mono-layer ϕ_{n-n}^{zz} is -6.1 eV/Å^2. When a vacancy is introduced, ϕ_{n-n}^{zz} is strongly affected. More precisely, for the 2-coordinated C atoms the average value is only -3.03 eV/Å^2. The origin of the ϕ_{n-n}^{zz} variations between the 2-coordinated atoms is discussed in the Appendix. As shown in the appendix the average value is robust and the fluctuations reduce as the supercell size increases. As we move away from the vacancy we rapidly recover the inter-atomic force constant of the pristine compound. Note, that this is also the case for the other couplings. A vacancy has the strongest effect on the nearest-neighbour IFC of the 2-coordinated C atoms, for larger distances between C atoms (beyond nearest-neighbours), the IFCs are much less affected. Thus, for the calculation at finite concentration of randomly distributed vacancies of the phonon lifetimes and transport properties, a vacancy is treated as follows: (i) a removal of a C atom and all corresponding bonds and (ii) a reduction by a factor 2 of the nearest neighbour IFC of the 2-coordinated C atoms for both in

and out of plane modes. Note that because of the random positions of the vacancies, in large systems considered here, there are many occurrences of double C-vacancies and even triple C-vacancies. This would in principle require the calculations of the IFC for these configurations but this goes beyond the scope of the present study. We should also mention, in contrast to what has been reported recently in a semi-empirical theoretical study,[13] that the $\phi_{n-n}^{\alpha\beta}$ are not enhanced by a factor 2 but strongly suppressed as revealed by our first principle calculations.

To obtain the vacancy induced multiple scattering contribution to the phonon scattering rate, we evaluate numerically on large systems (between 3.10^5 and 10^6 C atoms) the phonon dynamical spectral function. For such systems, finite size effects were found negligible. Note that this function is directly accessible from inelastic neutron scattering experiments. For a fixed concentration of vacancies and given configuration of disorder (random positions of the vacancies), the dynamical spectral function reads (further details are available in the Appendix),

$$A_s(\mathbf{q},\omega) = -\frac{2}{\pi}\omega\Im(G_s(\mathbf{q},\omega)), \qquad (1)$$

where

$$G_s(\mathbf{q},\omega) = \lim_{\eta\to 0} < \mathbf{q}, s| \left[(\omega^2 + i\eta)\hat{\mathbf{1}} - \hat{\mathbf{D}}\right]^{-1} |\mathbf{q}, s >, \quad (2)$$

where $\hat{\mathbf{D}}$ is the dynamical matrix and $|\mathbf{q}, s >$ is a Bloch state with momentum $\mathbf{q}$ and polarisation vector $\mathbf{e}_s$, and η is a small imaginary part. The matrix element $D_{\mathbf{ij}}^{\alpha\beta} = \frac{\phi_{\mathbf{ij}}^{\alpha\beta}}{\sqrt{m_{\mathbf{i}}m_{\mathbf{j}}}}x_{\mathbf{i}}x_{\mathbf{j}}$, where $x_{\mathbf{i}} = 0$ if the site $\mathbf{i}$ is occupied by a vacancy, otherwise $x_{\mathbf{i}} = 1$. In addition, for 2-coordinated atoms $\phi_{\mathbf{ij}}^{\alpha\beta}$ is half of its value in the pristine compound for nearest-neighbour IFC only. For a given $\mathbf{q}$ of the BZ, the peaks in $A_s(\mathbf{q},\omega)$ provide both the energy of the phonon modes and the lifetimes that correspond to the inverse of the full width at half maximum (FWHM) of the peaks. To extract reliably and accurately the phonon peak positions and more particularly the FWHM that are strongly η dependent for low energy modes, the calculations are performed using the powerful iterative Chebyshev Polynomial Green's Function approach (CPGF).[27,28] A similar methodology involving Chebyshev Polynomials to expand the time evolution operator has been developed earlier to address the dc conductivity in quasi crystals.[29] Note that performing a direct exact diagonalization of the disordered dynamical matrix, would require a large amount of both memory and CPU time. In particular the CPU time scales as N^3, where N is the total number of C atoms. In contrast, the calculation using CPGF scales linearly with the system size and the memory required is small, because there is no need to store large matrices. We should emphasize that, within CPGF the treatment of the disorder is exact. Thus, quantum interferences and localization phenomena are fully included.

Fig. 1(right) represents the disorder averaged dynamical spectral function for both in plane and out of plane
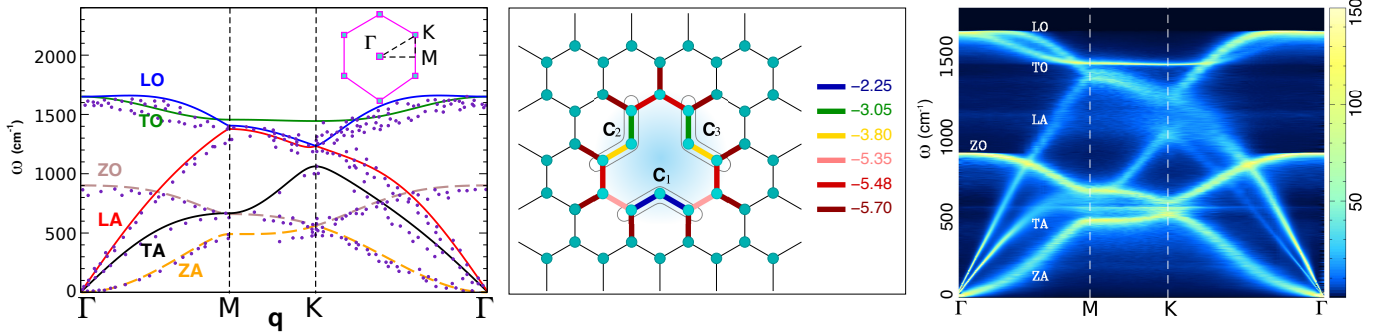
Figure 1: (left) Calculated phonon dispersions in pristine graphene along the Γ-M-K-Γ path (continuous lines) for LA, TA, LO, TO, ZA and ZO branches. The dotted symbols are experimental data from Ref.[30–32]. (middle) *ab initio* calculated nearest-neighbour inter-atomic force constants for the ZA and ZO modes in the vicinity of a vacancy (in eV/Å^2). (right) 2D color plot of the calculated averaged phonon dynamical spectral function $A_s(\mathbf{q}, \omega)$ in the presence of 5% of vacancies. The chosen polarisation for the in-plane modes is $\mathbf{e}_s = \frac{1}{\sqrt{2}}(\mathbf{e}_x + \mathbf{e}_y)$.

modes and a concentration of vacancies set to $x = 5\%$. Note that, because of the large system sizes considered here, a few configurations of disorder are enough to get reliable statistical average. At most 5 configurations of disorder are enough to get reliable values for both the phonon dispersion and the FWHM, with weak fluctuations from one configuration to the other. In addition, in this figure, a small finite η has been kept for the sake of visibility. However, in what follows and in order to properly extract the exact disorder contribution to the phonon lifetime the limit $\eta \to 0$ will be properly carried out. In the vicinity of the Γ point the phonon modes are well defined, but the ZA modes appear to have a much broader width than that of the in-plane acoustic modes. As we move away, along the Γ-M or Γ-K path, first the phonon width of the acoustic modes increases significantly (lifetime reduces) and then becomes almost constant. The case of the optical modes is slightly different. In particular, for TO branch, the width first increases rapidly then reaches a maximum and as we approach the zone boundary it decreases again. Along the M-K path, ZA, ZO and especially TO modes are very sharp in contrast to LA, TA and LO modes. In this region, it is difficult to separate LO and LA modes. It is worth mentioning two other interesting features: a well defined vacancy induced flat band located at about 500 cm^{-1} and the disappearance (fuzzy region) of the phonon modes around 1200 cm^{-1} in the vicinity of the K point.

Let us now discuss the effects of the vacancy concentration (x) on phonon dispersions, extracted from the peak positions in the spectral function. We choose here to focus our attention on the Γ-M direction. The results for the acoustic modes LA, TA and ZA are depicted in Fig. 2. We first observe that both dispersions and velocities of LA and TA modes are weakly affected, the effects start to be visible for relatively large vacancy concentration of the order of 10%. In contrast, the situation is very different for the ZA branch. For large values of the momentum $|\mathbf{q}|$, the dispersion is insensitive to the vacancy

concentration. However, in the vicinity of the Γ point the dispersion goes from quadratic to linear. The long wavelength modes develop a finite velocity v_{ZA} that depends on x. For instance, if we set $x = 5\%$, we find that v_{ZA} is as large as $0.15\, v_{LA}$. As clearly shown in the inset, the region of linear dispersion rapidly increases with the concentration of defects.

We now propose to analyse the effects of vacancies on the phonon modes FWHM denoted $\Gamma(\omega)$. $A_s(\mathbf{q}, \omega)$ has been calculated in the whole BZ. Typically 200 to 300 $\mathbf{q}$-points uniformly distributed over the BZ have been targeted. Note that the number of Chebyshev polynomials (CP) considered were typically of the order of 2.10^4 for $\mathbf{q}$-points far from the BZ center (see appendix B for the details). However, for the acoustic modes in the vicinity of the BZ center, because of the tiny values of the FWHM, it was necessary to include up to 3.10^6 CP to get converged results denoted "highly accurate calculations". $\Gamma(\omega)$ (rescaled by $x(1-x)$) as a function of the phonon mode energy is plotted in Fig. 3 for both LA and TA branches. The highly accurate calculations for the low energy modes in the ΓM direction are also shown. First, we observe for both branches a non monotonic behaviour of $\Gamma(\omega)$. We also find for $\omega \le 400$ cm^{-1} that the data points obtained for various vacancy concentrations lie on the same curve. Beyond 400 cm^{-1}, we observe, for a given energy, larger fluctuations around the average value. They are relatively small for the LA branch, of the order of 10 %. In contrast, they are much larger for the TA modes. For instance, for $\omega = 600$ cm^{-1} the fluctuations are of the order of 30 %. However, beyond 700 cm^{-1} the fluctuations are strongly suppressed. In addition, for $\omega \le 500$ cm^{-1}, the FWHM is found cubic in energy: $\Gamma_\lambda(\omega) = x(1-x)\frac{\omega^3}{\omega_{0,\lambda}^2}$ where $\omega_{0,\lambda} = 288$ cm^{-1} and 236 cm^{-1} respectively for $\lambda = $ LA and TA. The cubic power law found here is in agreement with perturbation theory (PT) that gives $\Gamma_\lambda^{PT}(\omega) = x\frac{\pi}{2}(\frac{\Delta M}{M})^2\omega^2\rho_\lambda(\omega)$, ΔM is the mass variation of the substituted atom and $\rho_\lambda(\omega)$ denotes the phonon density of states in the pristine compound.[33]
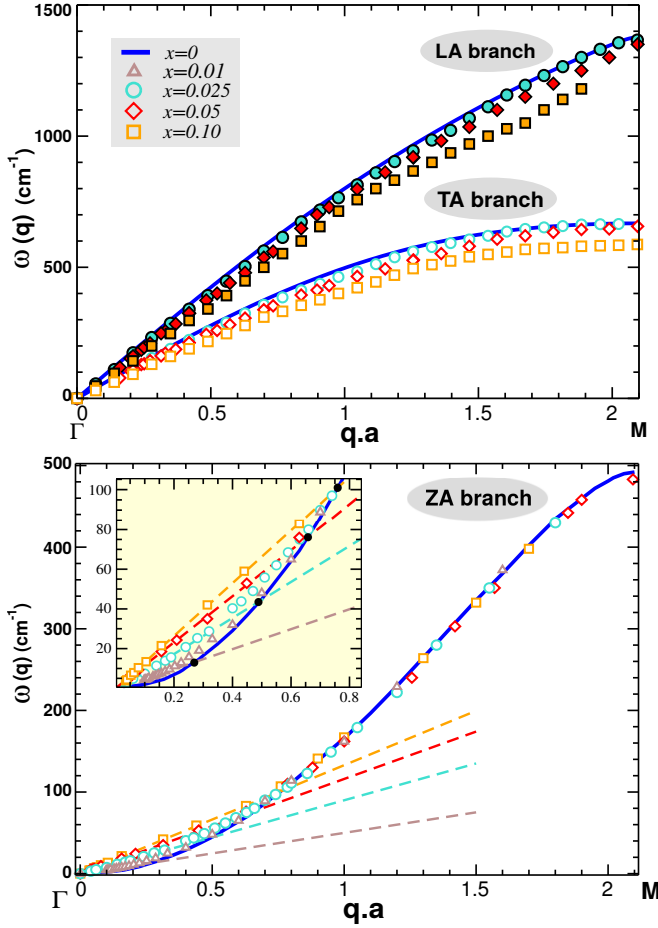
Figure 2: (top) LA and TA phonon dispersions along the Γ-M direction for various concentrations of vacancies ranging from $x = 0$ to 0.1. (bottom) ZA phonon dispersion in the ΓM direction for the same concentrations. The dashed lines correspond to linear fits for the long wavelength phonons. The inset shows a zoom of this region.

Figure 3: (top) LA phonon full width at half maximum (rescaled by $x(1-x)$) at $T = 0$ K as a function of the phonon energy ω for $x = 0.025$, 0.05 and 0.1. A grid of 200 to 300 **q**-points uniformly distributed over the whole Brillouin zone has been used. The filled symbols correspond to highly accurate calculations in the Γ-M direction (see text). The continuous line is a cubic fit of this set of data up to 500 cm^{-1}. (bottom) Same as in the top figure but for TA branch.

In the particular case of vacancies $\frac{\Delta M}{M} = -\frac{M_a}{M} - 2 \approx -3$, M_a being the mass of the missing atom and M the average mass per atom, -2 accounts for the potential energy of the missing linkage.[34,35] For LA and TA modes the density of states is $\rho_\lambda(\omega) = \frac{\Omega}{2\pi v_\lambda^2}\omega$ where Ω is the primitive cell area. The comparison between PT and our exact results leads to $\Gamma_{LA}^{PT} \approx 0.018\,\Gamma_{LA}$ and $\Gamma_{TA}^{PT} \approx 0.03\,\Gamma_{TA}$. Thus, perturbation theory drastically underestimates the vacancy contribution to the scattering rate. This is not surprising considering the non-perturbative nature of such defects compared to isotopic disorder. Note that in a recent study[22] devoted to thermal transport in irradiated graphene, a value of $\left(\frac{\Delta M}{M}\right)^2$ of the order of 590 instead of 9 was found necessary to reproduce the experimental data. This is entirely consistent with our finding that LA scattering rate is about 55 times larger than that predicted by PT.

The case of the ZA branch is even more interesting. $\Gamma(\omega)$ for the ZA branch is plotted in Fig. 4. First, after
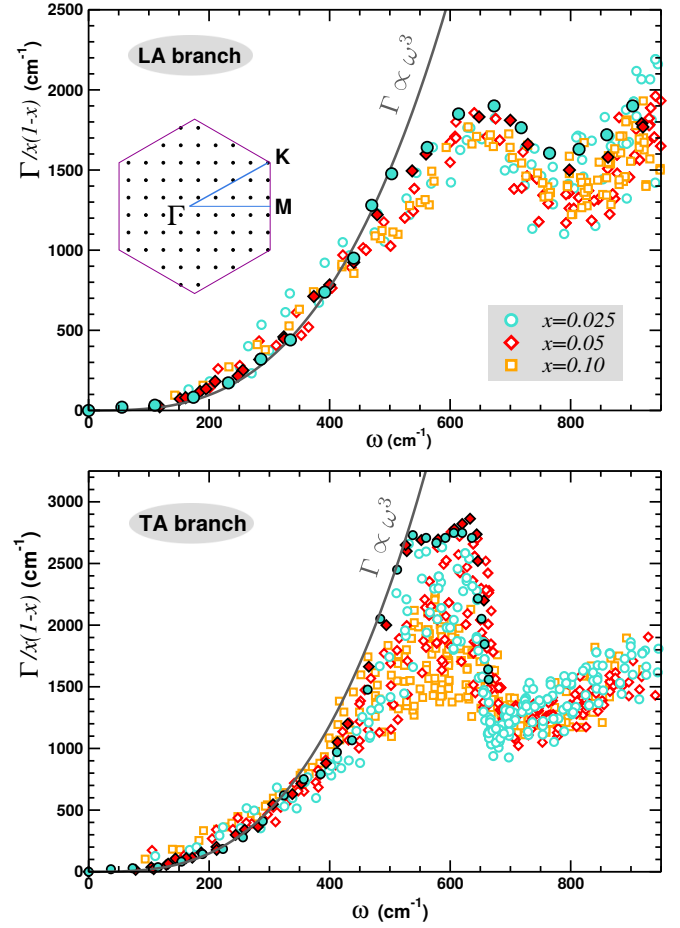
rescaling, the data points lie on a single curve as seen previously for in plane modes. The behaviour is non monotonic, $\Gamma(\omega)$ exhibits a maximum at about 200 cm^{-1} and a strong decrease as we approach the BZ boundary (M and K points). The fluctuations for a given ω are found relatively small, at most of the order of 10% to 15% around the average value. Unexpectedly, as we introduce vacancies, we find a linear behaviour of Γ_{ZA} as a function of the mode energy in the vicinity of the BZ center. The fluctuations are very small in this region as clearly seen in the inset. A linear fit for $\omega \leq 100$ cm^{-1} leads to $\Gamma_{ZA}(\omega) = 20\,x(1-x)\,\omega$. This linear scaling of the ZA width in the long wavelength regime means that these modes are marginal since $\lim_{\omega \to 0} \frac{\Gamma_{ZA}}{\omega} = 20\,x(1-x)$. For well defined excitations, one expects this ratio to be zero. Furthermore, $\Gamma_{ZA}(\omega) \geq \omega$ for $x \geq 0.05$, hence the phonon quasi-particles are not well defined in this range of vacancy concentrations. These findings are in
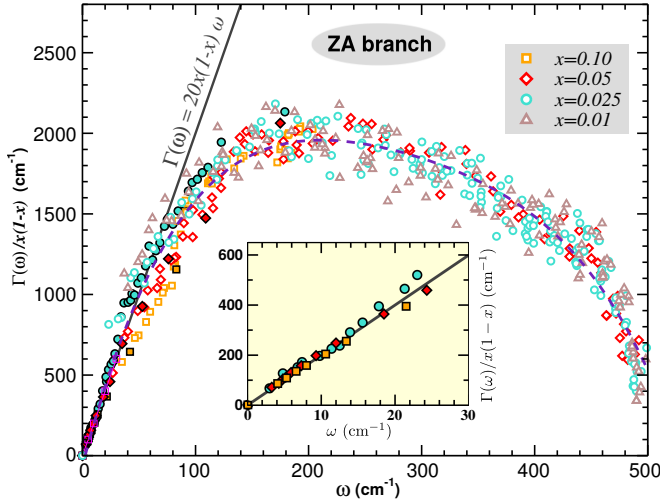
Figure 4: ZA phonon full width at half maximum (rescaled by $x(1-x)$) at $T = 0$ K as a function of the phonon energy ω for $x = 0.01, 0.025, 0.05$ and 0.1. A grid of 200 to 300 **q**-points uniformly distributed over the whole Brillouin zone has been used. The filled symbols correspond to highly accurate calculations in the Γ-M direction (see text). The continuous line is a linear fit for the low energy modes (see inset).

Figure 5: Thermal conductivity κ in W.m.$^{-1}$K^{-1} as a function of temperature for various concentrations of vacancies ranging from 0 to 0.01 (continuous lines). The symbols (circles, stars and diamonds) are experimental measurements extracted from Refs.[4,7,37]. The inset represents the variation of the room temperature κ as a function of x, the blue continuous line is a fit for $x \geq 10^{-5}$.

strong contrast with perturbation theory. Indeed, it is expected that $\Gamma_{ZA}^{PT}(\omega) = x(\frac{\Delta M}{M})^2 \frac{\Omega}{8D}\omega^2$ where D is the curvature of the ZA branch in the pristine compound, i.e. $\omega(\mathbf{q}) = D|\mathbf{q}|^2$ in the long wavelength limit. Therefore, the prediction of a quadratic power law from perturbation theory is inconsistent with the exact numerical results. For example, for $\omega = 50$ cm^{-1} and 100 cm^{-1} we find $\frac{\Gamma_{ZA}^{PT}}{\Gamma_{ZA}} = 0.045$ and 0.09 respectively. Once again, perturbation theory severely overestimates the phonon lifetime and hence the mean free path of the ZA phonon modes in the presence of vacancies. Because the thermal conductivity is dominated by the ZA modes in both pristine graphene and in the presence of C isotopes,[36] we naturally expect in the calculation of κ a strong deviation from PT as vacancies are introduced.

III. EFFECTS OF VACANCIES ON THE THERMAL CONDUCTIVITY

Linearized Boltzmann Transport Equation (BTE)[38,39] is a frequently used and efficient theoretical approach to address the thermal conductivity in 2D and 3D materials. In the great majority of studies, and because solving exactly the BTE is more cumbersome,[40,41] the relaxation time approximation (RTA) is often assumed. However, comparative studies have revealed that RTA calculated thermal conductivity is often much smaller than the full BTE solution in 3D.[42–45] The discrepancy is even stronger in 2D compounds such as pristine or natural graphene monolayer.[14,36,46] The origin of the discrepancy is the fact that within RTA, Umklapp (U) and Normal
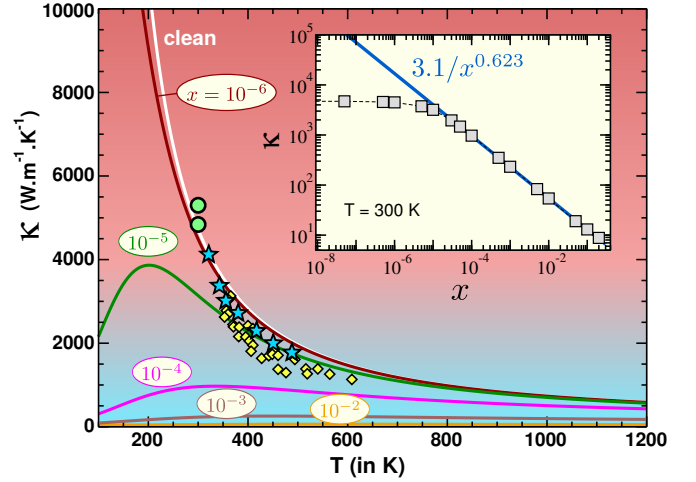
(N) phonon-phonon scattering processes are treated on equal footings, as resistive. However, N processes are not resistive, the thermal conductivity is expected to diverge in the absence of U scattering. There is an alternative to full BTE that can be implemented more easily and corrects the shortcomings intrinsic to the RTA approach. Several decades ago, Callaway proposed a theory that allows U and N processes to be treated separately.[47–49] It has been found that the Callaway theory leads to thermal conductivities that agree very well with the full BTE approach in 3D systems such as Si[50] and even in graphene.[51] Here, we propose to address the effects of the vacancies on thermal conductivity using the Callaway approach (see details in the Appendix. Within this approach the thermal conductivity in the α-direction reads,

$$\kappa^{\alpha} = \kappa_{RTA}^{\alpha} + \Delta\kappa^{\alpha}, \qquad (3)$$

the first term is the RTA contribution and the second one is the correction due to the appropriate separation between resistive and non-resistive processes. κ_{RTA}^{α} is given by,

$$\kappa_{RTA}^{\alpha} = \frac{1}{k_B T^2} \frac{1}{N\Omega\delta} \sum_{\mathbf{q},\lambda} (\hbar\omega_{\lambda})^2 (v_{\lambda}^{\alpha})^2 \times$$
$$\tau_{\lambda}^{tot} f_{\lambda}^0 (f_{\lambda}^0 + 1), \qquad (4)$$

δ is the separation of carbon planes in graphite, f_{λ}^0 is the Bose-Einstein distribution for the λ-branch and v_{λ}^{α} the velocity in the α-direction. According to Mathiessen's rule the total phonon lifetime is $1/\tau_{\lambda}^{tot} = 1/\tau_{\lambda}^N + 1/\tau_{\lambda}^U + 1/\tau_{\lambda}^{dis}$. We remind that the disorder contribution is $\tau_{\lambda}^{dis} = \frac{\hbar}{\Gamma_{\lambda}}$. The full expression of $\Delta\kappa^{\alpha}$ is given in the Appendix. For the thermal conductivity calculations, we

use the *ab initio* results for τ_λ^N and τ_λ^U as found in ref.[15]. For τ_λ^{dis}, we use the analytical forms discussed previously (see details in the Appendix). In Fig. 5, the average thermal conductivity $\kappa = (\kappa^x + \kappa^y)/2$ (see eq.3) is plotted as a function of temperature for various concentrations of vacancies. In the clean limit ($x = 0$), we find very high values of the thermal conductivity and because of the presence of the U-processes, we observe a $1/T$ suppression of κ. As we introduce a very small amount of vacancies of the order of $x = 10^{-5}$ only, the effects are dramatic below 200 K. At room temperature, κ is already reduced by 40 % and the suppression is even stronger for $x = 10^{-4}$. Indeed, for this concentration, $\kappa = 1000$ W.m.$^{-1}$K^{-1} at room temperature, five times smaller than that of pristine graphene. As we increase the vacancy concentration to 0.1%, the thermal conductivity falls to $\kappa = 200$ W.m.$^{-1}$K^{-1}, 25 times smaller than that of pristine. The variation of κ at 300 K is plotted in the inset as a function of x and reveals a crossover around $x = 10^{-5}$. Below this concentration, κ is weakly sensitive to the defects concentration, and above, κ decreases rapidly with a power law decay $\kappa \propto 1/x^{0.623}$. There is no simple way to anticipate such an exponent. Let us now compare our results to experimental measurements.[4,7,37] At room temperature, in the pristine limit, we obtain $\kappa = 4800$ W.m.$^{-1}$K^{-1} which is in very good agreement with the highest experimental values of the thermal conductivity ever reported.[4] The agreement with the other data sets beyond room temperature is also relatively good. The measured values are consistent with an extremely low concentration of defects of the order of $x = 10^{-6}$ to 10^{-5} suggesting that the samples should be of good quality. Notice that, the agreement between theory and experiments, in the pristine case, has already been achieved in the full BTE calculations of Refs.[14,36]. Finally, it is interesting to comment on the validity of the RTA approximation. The study of $\frac{\Delta \kappa}{\kappa_{RTA}}$ as a function of T (see figure in the Appendix) has revealed that the correction to RTA is extremely large and even dominant for the lowest concentrations of vacancies, typically when $x \leq 10^{-4}$. However, when the vacancy concentration is large enough beyond 0.1% of the C atoms, the correction becomes very small.

IV. CONCLUSION

Combining state of the art *ab initio* approaches with a full and exact treatment of the disorder, we have addressed the impact of vacancies on phonon thermal transport in graphene. It has been found that the vacancy induced multiple scattering contribution to phonon lifetimes are much larger than predicted by second order perturbation theory. Furthermore, vacancies have drastic effects on both dispersion and lifetime of ZA modes. The ZA dispersion becomes linear in the vicinity of the Brillouin zone center and the vacancy induced scattering rate is linear in energy instead of the quadratic behaviour often assumed. We have also shown that the vacancies have dramatic effects on the thermal conductivity calculated beyond the relaxation time approximation. A mere 0.1% of vacancies leads to a spectacular 95% suppression of the thermal conductivity at room temperature. These findings contribute to a better understanding of thermal transport in 2D materials and could be promising for high-efficiency thermoelectric power generation as the high lattice conductivity in natural graphene is the major obstacle. It is also worth noticing that our methodology is very general, it could easily incorporate other features such as extended defects, porosity and nanostructuring.

V. APPENDIX

A. *ab initio* calculations of the Interatomic Force Constants

The *ab initio* calculations are performed with the DFT package SIESTA based on atomic orbitals.[25] The exchange-correlation functional used here corresponds to the generalized gradient approximation as proposed by Perdew, Burke & Ernzerhof.[52] However, the local density approximation leads to similar results. Troullier-Martin norm-conserving pseudopotentials[53] are used. The basis corresponds to a double-ζ-polarized basis optimized with the simplex tool of the SIESTA package. All the atomic structures were optimized up to forces less than 10^{-4} eV/Å and to an hydrostatic pressure smaller than 10 bar. Finally, a Monkhorst-pack of $10 \times 10 \times 1$ k-points is used for the calculations along with a mesh cutoff used to compute the Hartree potential of 600 Ry.

The IFC, $\phi_{ij}^{\alpha\beta}$, were calculated by the finite displacement method. The displacement amplitude was 0.04 Bohr. Note that, we use the local constraint $\phi_{ii}^{\alpha\beta} = -\sum_{j \neq i} \phi_{ij}^{\alpha\beta}$ that ensures that no force results from a global translation of the whole system.

In the presence of a C vacancy, two different supercells have been used to compute the inter atomic force constants. First, we have considered a large rectangular supercell with dimensions 21.3 Å $\times$24.6 Å (199 C atoms) and second a smaller trigonal supercell that contains 97 atoms. In both cases, the nearest-neighbours IFC (ϕ_{n-n}^{zz}) exhibit the same axial symmetry (y-axis) as that of the chosen supercell. The average value of the ϕ_{n-n}^{zz} of the 2-coordinated atoms is -3.03 eV/Å^2 for the smallest supercell and -2.82 eV/Å^2 for the largest. The fluctuations around the average, were about 0.4 eV/Å^2 and 0.8 eV/Å^2 respectively for the rectangular and trigonal supercells. These fluctuations originate from the non-symmetric free relaxation of the C atoms in the supercells. The value of the fluctuations decreases strongly with the supercell size typically as the inverse of the number of C atoms, but the average value is only weakly affected. Hence, this validates our procedure to consider the average value for the IFC of the 2-coordinated C atoms in our calculations. The angles involving C_2 and C_3 of Fig. 1 in the

manuscript are close to 121°, in contrast, that of C_1 is around 126° for the largest supercell, and the distance were slightly shorter for the bonds involving C_1.

B. The Chebyshev Polynomials Green's Function

In the presence of the C vacancies, the matrix elements of the 3N × 3N (N total number of C atoms) disordered dynamical matrix $\hat{\mathbf{D}}$ read,

$$D_{\mathbf{ij}}^{\alpha\beta} = <\mathbf{i}, \alpha|\hat{\mathbf{D}}|\mathbf{j}, \beta> = \frac{\phi_{\mathbf{ij}}^{\alpha\beta}}{\sqrt{m_\mathbf{i} m_\mathbf{j}}} x_\mathbf{i} x_\mathbf{j}, \quad (5)$$

where α = x, y and z, $\mathbf{i}$ and $\mathbf{j}$ are the site positions. The random variable x_i is zero if the site is occupied by a vacancy, otherwise 1. In addition for 2-coordinated C atoms and if $\mathbf{i}$ and $\mathbf{j}$ are nearest-neighbours $\phi_{\mathbf{ij}}^{\alpha\beta}$ is half of its value in the pristine compound. We define the plane wave state,

$$|\mathbf{q}, \alpha> = \frac{1}{\sqrt{N}} \sum_\mathbf{i} e^{i\mathbf{q} \cdot \mathbf{r}_i} |\mathbf{i}, \alpha>, \quad (6)$$

where the sum runs over the sites occupied by C atoms. For in plane modes, for a chosen polarisation vector $\mathbf{e}_s = \cos(\theta_s).\mathbf{e}_x + \sin(\theta_s).\mathbf{e}_y$, we define $|\mathbf{q}, s> = cos(\theta_s)|\mathbf{q}, x> + \sin(\theta_s)|\mathbf{q}, y>$. Hence, $\mathbf{e}_s = (\frac{q_x}{|\mathbf{q}|}, \frac{q_y}{|\mathbf{q}|})$, $(\frac{-q_y}{|\mathbf{q}|}, \frac{q_x}{|\mathbf{q}|})$ and $(\frac{1}{\sqrt{2}}, \frac{1}{\sqrt{2}})$ for respectively longitudinal, transverse and (1,1)-axis polarisation. For the out of plane modes (ZO, ZA) $\mathbf{e}_s = \mathbf{e}_z$.

To calculate the dynamical spectral function, we fix the polarization and choose a vector $\mathbf{q}$ in the discretized BZ. The procedure described in what follows is repeated for a large number of $\mathbf{q}$. The phonon dynamical spectral function is given by,

$$A_s(\mathbf{q}, \omega) = -\frac{2}{\pi}\omega.\Im(G_s(\mathbf{q}, \omega)), \quad (7)$$

where the Green's function reads,

$$G_s(\mathbf{q}, \omega) = \lim_{\eta \to 0} <\mathbf{q}, s|\left[z\hat{\mathbf{1}} - \hat{\mathbf{D}}\right]^{-1}|\mathbf{q}, s>, \quad (8)$$

where $z = \omega^2 + i\eta$, $G_s(\mathbf{q}, \omega)$ is calculated using the Chebyshev Polynomials Green's Function method (CPGF) as described in details in Refs[27,28]. The starting point is a rescaling of the dynamical matrix such that the spectrum is contained in the interval [-1, 1], in fact [0, 1] here. We define the rescaled matrix $\mathbf{D}_r = \hat{\mathbf{D}}/a$, $\omega_r^2 = \omega^2/a$ and $\eta_r = \eta/a$, a denotes the rescaling factor. The crucial step is the fact that the rescaled Green's function can be expanded exactly in terms of the Chebyshev polynomials T_n,[27]

$$\left[z_r\hat{\mathbf{1}} - \hat{\mathbf{D}}_\mathbf{r}\right]^{-1} = \sum_{n=0}^{\infty} g_n(z_r)T_n(\hat{\mathbf{D}}_\mathbf{r}), \quad (9)$$

where $z_r = \omega_r^2 + i\eta_r$,

$$g_n(z) = \frac{2i^{-1}}{1 + \delta_{n,0}} \frac{(z - i\sqrt{1 - z^2})^n}{\sqrt{1 - z^2}}. \quad (10)$$

$T_n(\hat{\mathbf{D}}_r)$ obeys the recursion relation,

$$T_{n+1}(\hat{\mathbf{D}}_r) = 2\hat{\mathbf{D}}_r.T_n(\hat{\mathbf{D}}_r) - T_{n-1}(\hat{\mathbf{D}}_r), \quad (11)$$

with $T_0(\hat{\mathbf{D}}_r) = \hat{\mathbf{1}}$ and $T_1(\hat{\mathbf{D}}_r) = \hat{\mathbf{D}}_r$. This implies that eq.(8) becomes,

$$G_s(\mathbf{q}, \omega) = \lim_{\eta \to 0} \frac{1}{a} \sum_{n=0}^{\infty} \mu_n(\mathbf{q}, s)g_n(z_r), \quad (12)$$

where,

$$\mu_n(\mathbf{q}, s) = <\mathbf{q}, s|T_n(\hat{\mathbf{D}}_r)|\mathbf{q}, s>, \quad (13)$$

are called the moments.

In practice, the series of eq.(12) is truncated when the convergence for a chosen value of η is reached within a certain accuracy. The efficiency and power of the CPGF method is that the moments $\mu_n(\mathbf{q}, s)$ are obtained iteratively using the recursion relation of the Chebyshev polynomials without any need to store large matrices. Note that, to extract reliably the C vacancy contribution to the phonon lifetime, $\sqrt{\eta}$ has to be much smaller than the full width at half maximum of the peaks in the spectral function. As a consequence, a large number of moments is required as we approach the Γ point in the BZ.

C. The Callaway theory

The full and detailed derivation of the Callaway method can be found in Refs.[47–49]. Here, we just summarize the main results. The total conductivity in the α-direction can be written,

$$\kappa^\alpha(T) = \kappa_{RTA}^\alpha(T) + \Delta\kappa^\alpha(T), \quad (14)$$

where, the RTA contribution is,

$$\kappa_{RTA}^\alpha = \frac{1}{k_B T^2} \frac{1}{N\Omega\delta} \sum_{\mathbf{q}, \lambda} (\hbar\omega_\lambda)^2 (v_\lambda^\alpha)^2 \times \\ \tau_\lambda^{tot} f_\lambda^0(f_\lambda^0 + 1), \quad (15)$$

N is the total number of unit cells, λ the mode index (LA, TA, ZA), Ω the primitive cell area, δ the distance between graphene sheets in graphite, f_λ^0 is the Bose distribution, $\hbar\omega_\lambda$ the mode energy, v_λ^α its velocity in the α-direction and τ_λ^{tot} the inverse of the total scattering rate for the branch λ. According to Mathiessen's rule the total phonon lifetime is,

$$1/\tau_\lambda^{tot} = 1/\tau_\lambda^N + 1/\tau_\lambda^U + 1/\tau_\lambda^{dis}. \quad (16)$$

The first step consists in replacing in the standard Boltzmann equation the collision rate by,

$$\left(\frac{\partial f_\lambda}{\partial t}\right)_c = \frac{f_\lambda^d - f_\lambda}{\tau_N} + \frac{f_\lambda^0 - f_\lambda}{\tau_R}, \qquad (17)$$

f_λ^d is the drifted distribution function, and we have defined the scattering rate for resistive processes, $1/\tau_\lambda^R = 1/\tau_\lambda^U + 1/\tau_\lambda^{dis}$. Only the resistive processes tend to bring f_λ back to its equilibrium value. The drifted distribution f_λ^d is defined by

$$f_\lambda^d = \frac{1}{e^{\beta(\omega_\lambda(\mathbf{q}) - \mathbf{v}_d \cdot \mathbf{q})} - 1}, \qquad (18)$$

where we have introduced as a Lagrange multiplier the drift velocity $\mathbf{v}_d$. This quantity is determined by the condition that the normal processes conserve the momentum. By following step by step Callaway's derivation we find,

$$\Delta\kappa^\alpha(T) = \frac{(A^\alpha(T))^2}{B^\alpha(T)}, \qquad (19)$$

where the numerator $A^\alpha(T) = \sum_\lambda A_\lambda^\alpha(T)$ and,

$$A_\lambda^\alpha(T) = \frac{1}{k_B T^2} \frac{1}{N\Omega\delta} \sum_\mathbf{q} \frac{\tau_\lambda^{tot}}{\tau_\lambda^N} \hbar\omega_\lambda v_\lambda^\alpha q^\alpha \times$$
$$f_\lambda^0(f_\lambda^0 + 1), \qquad (20)$$

and the denominator $B^\alpha(T) = \sum_\lambda B_\lambda^\alpha(T)$ and,

$$B_\lambda^\alpha(T) = \frac{1}{k_B T^2} \frac{1}{N\Omega\delta} \sum_\mathbf{q} \frac{\tau_\lambda^{tot}}{\tau_\lambda^N \tau_\lambda^R} \times$$
$$(q_\lambda^\alpha)^2 f_\lambda^0(f_\lambda^0 + 1). \qquad (21)$$

To facilitate the calculations we replace the discrete sum over $\mathbf{q}$ by an integral over energy and thus we introduce Debye frequencies for LA, TA and ZA modes. This leads to,

$$A_\lambda^\alpha(T) = c_\lambda \frac{1}{\Omega\delta} \int_0^{\omega_{D\lambda}} \frac{\tau_\lambda^{tot}}{\tau_\lambda^N} \omega \rho_\lambda(\omega) \frac{\partial f^0}{\partial T} d\omega, \qquad (22)$$

where the coefficient $c_\lambda = 1/2$ for LA and TA branches and 1 for ZA. Similarly $B_\lambda^\alpha(T)$ can be rewritten,

$$B_\lambda^\alpha(T) = \frac{1}{2\hbar\Omega\delta} \int_0^{\omega_{D\lambda}} \frac{\tau_\lambda^{tot}}{\tau_\lambda^N \tau_\lambda^R} g_\lambda(\omega) \times$$
$$\rho_\lambda(\omega) \frac{\partial f^0}{\partial T} d\omega. \qquad (23)$$

The density of states is $\rho_\lambda(\omega) = \frac{\Omega}{2\pi v_\lambda^2}\omega$ for both LA and TA, and $\frac{\Omega}{4\pi D}$ for ZA. v_λ is the velocity at the Γ point for LA and TA, and D is the curvature of the ZA branch: in the long wavelength limit $\omega(\mathbf{q}) = D|\mathbf{q}|^2$ for the ZA mode. $g_\lambda(\omega) = \frac{\omega}{v_\lambda^2}$ for LA and TA, and $1/D$ for ZA. Note that,
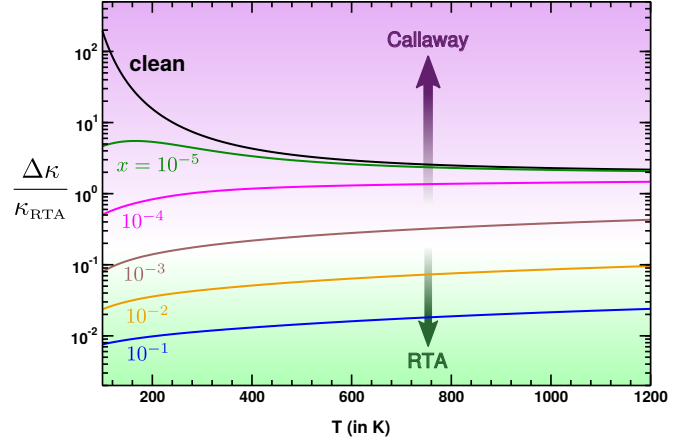

Figure 6: Callaway's correction to the total thermal conductivity over RTA contribution as a function of temperature, for various concentrations of C vacancies. The green area corresponds to negligible Callaway correction ("RTA regime") and the purple one to dominant Callaway correction.

in eq.(22) and (23) we have used the linear dispersion for LA and TA and the quadratic one for ZA.

To compute numerically the total conductivity as a function of temperature, we need the temperature dependence of τ_λ^N and τ_λ^U. We use the *ab initio* calculated scattering rate at room temperature (T_0) for both U and N processes ($\tau_{0,\lambda}^N$, $\tau_{0,\lambda}^U$) extracted from Ref.[15]. We make the following ansatz to have the full T variation of the scattering rates,

$$1/\tau_\lambda^N(T) = (1/\tau_{0,\lambda}^N)\frac{T}{T_0} \qquad (24)$$

and the Umklapp scattering rate is,

$$1/\tau_\lambda^U(T) = (1/\tau_{0,\lambda}^U)\frac{T}{T_0}e^{-\frac{\omega_{D\lambda}}{3}(\frac{1}{T} - \frac{1}{T_0})}. \qquad (25)$$

This ansatz is motivated by the fact that the form usually assumed for the N and U process are, $1/\tau_\lambda^N = \omega^a T^b$ and $1/\tau_\lambda^U \propto (1/\tau_\lambda^N)e^{-\frac{\omega_{D\lambda}}{cT}}$ where a = 1 or 2, b = 1, 2 or 3 and c is often set to 3.[47,54–56] For the vacancy concentration dependent scattering $1/\tau_\lambda^{dis}$ we use the results found in the present study.

We now discuss the importance of Callaway's correction to the thermal conductivity in graphene, in the presence of C vacancies. The results are depicted in Fig. 6. Let us first consider low vacancy concentrations ($x \leq 10^{-4}$). For this range of concentration, the correction $\Delta\kappa^\alpha(T)$ is important and even dominates. For instance the ratio $\Delta\kappa/\kappa_{RTA}$ is 1, 4.5 and 7.5 for $x = 10^{-4}$, 10^{-5} and for the pristine case at room temperature. On the other hand, when the vacancy concentration is large enough beyond 0.1% of the C atoms, the correction becomes very small, it is less than 15% of the RTA value. For $x = 1\%$ the correction to RTA represents only 5% of the total conductivity.

These results show that in the presence of a sufficient amount of C vacancies, beyond 0.1%, the RTA approach becomes appropriate for the evaluation of the thermal conductivity, provided that the scattering rates are calculated accurately.

[1] A.K. Geim and K.S. Novoselov, Nature Mater.**6, 183** (2007).

[2] A.C. Neto et al., Rev. Mod. Phys. **81,** 109 (2009).

[3] K.S. Novoselov et al., Nature **490,** 192 (2012).

[4] A. A. Balandin et al. Nano Lett.**8,** 902 (2008).

[5] S. Ghosh et al., Appl. Phys. Lett. **92,** 151911 (2008).

[6] W. Cai et al. Nano Lett.**10,** 1645 (2010).

[7] S. Chen et al., ACS Nano **5,** 321 (2011).

[8] R.S. Prasher et al., Phys. Rev. Lett. **102,** 105901 (2009).

[9] H. Sevinçli and G. Cuniberti, Phys. Rev. B **81,** 113401 (2010).

[10] J.H. Seol et al., Science **328,** 213 (2010).

[11] S. Ghosh et al., Nat. Mater. **9,** 151911 (2010).

[12] A. Weerasinghe, A. Ramasubramaniam and D. Maroudas, Appl. Phys. Lett. **11,** 163101 (2017).

[13] G. Xie et al. , Sci. Rep. **4,** 5085 (2014).

[14] G. Fugallo et al., Nano Lett. **14,** 6109 (2014).

[15] L. Pauletto, F. Mauri, M. Lazzeri, Phys. Rev. B **87,** 214303 (2013).

[16] L. Lindsay, D.A. Broido and N. Mingo, Phys. Rev. B **83,** 235428 (2011).

[17] W.J. Evans, L. Hu and P. Keblinski, Appl. Phys. Lett. **96,** 203112 (2010).

[18] S. Berber, Y-K Kwon and D. Tománek, Phys. Rev. Lett. **84,** 4613 (2000).

[19] G. Qin, Z. Qin, H; Wang and M. Hu, Computational Materials Science, **151,** 153 (2018).

[20] Z. G. Fthenakis, Z. Zhu, D. Tománek, Phys. Rev. B **89,** 125421 (2014).

[21] Z. G. Fthenakis, D. Tománek, Phys. Rev. B **86,** 125418 (2012).

[22] H. Malekpour et al., Nanoscale **8** 14608 (2016).

[23] Y. Y. Zhang, Y. Cheng, Q. X. Pei, C. M. Wang and Y. Xiang, Phys. Lett. A **376** 3668 (2012).

[24] A. Bagri, S.-P. Kim, R. S. Ruoff and V. B. Shenoy, Nano Lett.**11,** 3917 (2011).

[25] J. M. Soler et al. J. Phys. Condens. Matter, **14,**2745 (2002).

[26] C. A. Polanco and L. Lindsay, Phys. Rev. B **97,** 014303 (2018).

[27] A. Ferreira and E. R. Mucciolo Phys. Rev. Lett. **115,** 106601 (2015)

[28] A. Weisse, G. Wellein, A. Alvermann and H. Feskhe, Rev. Mod. Phys. **78,** 275 (2006).

[29] S. Roche and D. Mayou, Phys. Rev. Lett. **79,** 2518 (1997).

[30] L. Wirtz et al., Solid State Comm. **131**, 141 (2004) and references therein.

[31] M. Mohr et al., Phys. Rev. B **76**, 035439 (2007).

[32] J. Maultzsch, S. Reich, C. Thomsen, H. Requardt, and P. Ordejón, Phys. Rev. Lett. **92**, 075501 (2004).

[33] S-i Tamura, Phys. Rev. B, **27** 858 (1983).

[34] C.A. Ratsifaritana and P.G. Klemens - Int. J. of Thermophys. **8**, 737 (1987).

[35] P. G. Klemens, Physica B, **263-264**, 102 (1999).

[36] L. Lindsay, D.A. Broido and N. Mingo, Phys. Rev. B, **89** 155426 (2014).

[37] D.L. Nika and A.A. Balandin J. Phys. Condens. Matter **24**, 233203 (2012).

[38] R.E. Peierls, Ann. Phys. (Leipzig), **395**, 1055 (1929).

[39] J.M. Ziman, *Electron and Phonons: The theory of transport phenomena in solids*, Oxford Univ. Press, Oxford, U.K. (2001).

[40] M. Omini and A. Sparavigna, Physica B, **212**, 101 (1995).

[41] M. Omini and A. Sparavigna, Phys. Rev. B, **53**, 9064 (1996).

[42] D.A. Broido, M. Malorny, G. Birner, N. Mingo and D.A. Stewart, Appl. Phys. Lett., **91**, 231922 (2007).

[43] K. Esfarjani, G. Chen and H.T. Stokes, Phys. Rev. B, **84** 085204 (2011).

[44] A. Ward, D.A. Broido, D.A. Stewart and G. Deinzer, Phys. Rev. B, **80** 125203 (2009).

[45] J. Carrete, W. Li, N. Mingo , S. Wang and S. Curtarolo, Phys. Rev. X, **4** 011019 (2014).

[46] L. Lindsay, D.A. Broido and N. Mingo, Phys. Rev. B, **82** 115427 (2010).

[47] J. Callaway, Phys. Rev. **113,** 1046 (1959).

[48] P. B. Allen, Phys. Rev. B **88**, 144302 (2013).

[49] J. Ma, W. Li and X. Luo, Phys. Rev. B **90**, 035203 (2014).

[50] A. Ward and D.A. Broido, Phys. Rev. B **81,** 085205 (2010).

[51] A. Cepellotti et al.,Nat. Comm. **5**, 3689 (2014).

[52] J.P. Perdew, K. Burke and M. Ernzehof, Phys. Rev. Lett., **77**, 3865 (1996).

[53] N. Troullier and J. L. Martin, Phys. Rev. B, **43,** 1993 (1991).

[54] M.G. Holland, Phys. Rev. **132**, 2461 (1963).

[55] D.T. Morelli, J.P. Heremans and G.A. Slack, Phys. Rev. B, **66**, 195304 (2002).

[56] G.P. Srivastava, *The Physics of Phonons* (Adam Hilger, Bristol, 1990).